A Teleconnection between the Reduction of Rainfall in Southwest Western Australia and North China

YUN LI

CSIRO Mathematics, Informatics and Statistics, CSIRO Climate Adaptation Flagship, Wembley, Western Australia, Australia

JIANPING LI AND JUAN FENG

State Key Laboratory of Atmospheric Sciences and Geophysical Fluid Dynamics, Institute of Atmospheric Physics, Chinese Academy of Sciences, Beijing, China

(Manuscript received 18 October 2011, in final form 17 June 2012)

ABSTRACT

Rainfall in both southwest Western Australia (SWWA) and North China (NC) has been declining substantially since the mid-1960s, which has led to a series of droughts in both regions since then. Using observed rainfall datasets in China and Australia and the NCEP reanalysis dataset during 1951–2008, it is found that the decline of SWWA rainfall occurs in early austral winter [May–July (MJJ)] while the reduction of NC rainfall is in late boreal summer [July–September (JAS)]. The relationship between SWWA MJJ rainfall and NC JAS rainfall during 1951–2008 is then examined, and it is found that a significant link exists between these two rainfall series with a correlation of 0.43 and this link remains after the data are detrended. In particular, this relationship accounts for up to 62% variance on interdecadal time scales, and seems to be driven by the poleward shift of the southern subtropical high ridge (SSHR) and the northern subtropical high ridge (NSHR) over longitudes 110°–150°E. The poleward shift of the SSHR may induce an anomalous anticyclone centered near the south Australian coast, resulting in anomalous easterlies of dry air to SWWA, while the poleward shift of the NSHR is associated with an anomalous anticyclone in East Asia near NC causing anomalous northeasterlies of dry air to NC. The poleward shift of SSHR/NSHR may be linked to the warming sea surface temperatures (SSTs) in the tropical Indian-western Pacific. The results herein suggest that the poleward shifts of the SSHR and the NSHR instigated by the warming SSTs in the tropical Indian–western Pacific may have partially contributed to the rainfall reduction in both regions.

1. Introduction

Southwest Western Australia (SWWA; southwest of the line joining 30°S, 115°E and 35°S, 120°E; Fig. 1) receives the bulk of its annual rainfall during the winter half of the year (i.e., May to October; Fig. 2). Since the mid-1960s, SWWA has experienced a substantial drying trend with a winter rainfall decrease of some 15%–25% (IOCI 2002), which as a result causes a 50% dam decrease inflow. This has attracted significant interest and attention, particularly in terms of possible causes and policy options in response to the decrease. Previous studies have identified a range of factors as potential or likely contributors to the rainfall decrease, including natural variability (Cai et al. 2005), land-use changes (Pitman et al. 2004), the Indian Ocean temperatures (England et al. 2006; Ummenhofer et al. 2008), and atmospheric circulation changes including the Antarctic Oscillation (AAO) or southern annular mode (SAM) (Rogers and Vanloon 1982; Gong and Wang 1999; Thompson and Wallace 2000; Marshall 2003; Nan and Li 2003; Marshall et al. 2004).

Particular attention has been given to SAM changes. The decline of SWWA rainfall is manifested as a reduction in high-intensity rainfall events (Li et al. 2005) and is accompanied by an upward trend of the SAM with increasing mean sea level pressure (SLP) in the midlatitudes (Li et al. 2005; Cai and Cowan 2006). This implies that austral winter rainfall over SWWA tends to decrease as a result of decreased cloudiness and

Corresponding author address: Dr. Yun Li, CSIRO Mathematics, Informatics and Statistics, Wembley WA 6913, Australia.
E-mail: yun.li@csiro.au

DOI: 10.1175/JCLI-D-11-00613.1

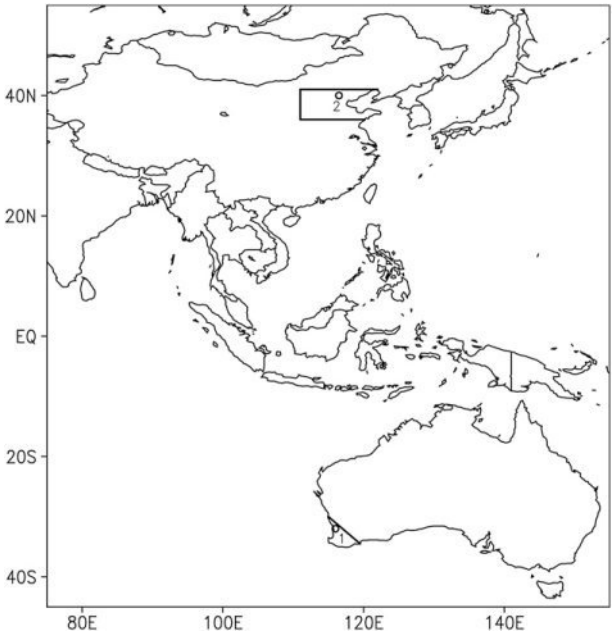

FIG. 1. Study area used for the two regional-scale study areas: 1) SWWA (southwest of the line joining 30°S, 115°E and 35°S, 120°E) and 2) North China (NC, the box area bounded by 36°–41°N and 111°–122°E with the right-hand side as the coastline). The stations at the capital city Perth in SWWA and Beijing in NC are shown as open dots.

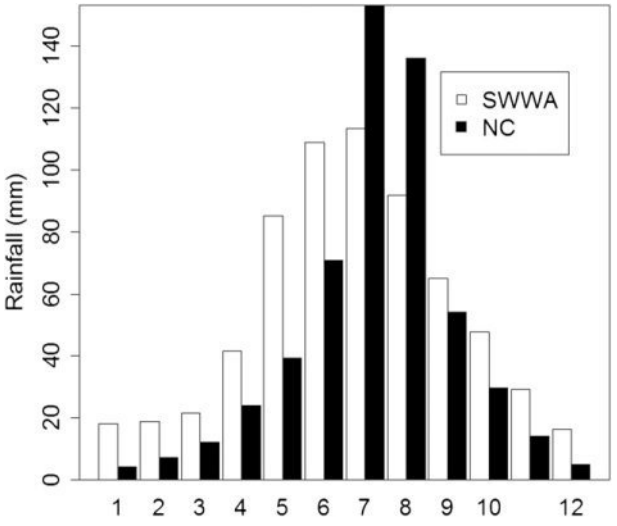

FIG. 2. Distributions of monthly rainfall totals over NC (black bar) and SWWA (white bar) during 1951–2008.

decreased westerly winds, a relationship that exists in both observations and the Commonwealth Scientific and Industrial Research Organisation (CSIRO) coupled global climate model (GCM) under increasing atmospheric CO_2 (Cai and Watterson 2002). The possibility of the rainfall reduction being a part of multidecadal variability of the SAM was found by using outputs of the CSIRO Mark 3 GCM in an experiment without CO_2 forcing (Cai et al. 2005). These results offer a support for the argument that the SAM may contribute to the drying trend over SWWA. As the SAM changes have been associated with climate forcing through stratospheric ozone depletion and carbon dioxide increase (Cai et al. 2003; Karoly 2003; Cai and Cowan 2006), this raises the prospect of anthropogenic contribution to the drought. However, the precise role of the SAM remains ambiguous (van Ommen and Morgan 2010); not least because the observed trend for the SAM is smallest in the winter season, when the precipitation impact is largest (Cai and Cowan 2006). For instance, there is little evidence that the SAM has contributed to seasonal precipitation change over Australia except for the summer seasons of the 1979–2004 period (Hendon et al. 2007). Meneghini et al. (2007) deduced that the cause of long-term reductions in winter rainfall (from 1965 onward) was unlikely to be due to trends in the SAM. The relationship between the SAM and SWWA rainfall during the 60-yr period (1948–2007) becomes insignificant when data for an extreme wet year coupled with an extreme negative wet year (1964) are excluded, indicating that the SAM SWWA winter rainfall relation does not statistically hold (Feng et al. 2010b).

Recently, Feng et al. (2010a) shows that a monsoon-like southwest Australia circulation (SWAC) may contribute to the rainfall decline in winter over SWWA. The driver of the SWAC may be the shift of the planetary-scale thermal convection (Zeng and Li 2002) associated with the shift of the subtropical high resulting in the reversal winds over SWWA, which may be linked to the poleward expansion of the Hadley circulation and the subtropical dry zone (Lu et al. 2007). Moreover, the SWWA draft has also been linked to snowfall increase in coastal East Antarctica by van Ommen and Morgan (2010). They found a significant inverse correlation between snowfall at Law Dome, East Antarctica, and rainfall in SWWA over the instrumental period, including the most recent decades. The driver of the observed inverse relation has been suggested to be the zonal wavenumber-3 circulation in the Southern Hemisphere (van Ommen and Morgan 2010). Here we report another significant positive correlation (or teleconnection) between the rainfall reductions over the past decades from 1951–2008 in SWWA and its teleconnected region (North China) in the Northern Hemisphere.

North China (NC; 36°–41°N, 111°–122°E; Fig. 1) is located at the northern part of the East Asian summer monsoon (EASM) region and receives the bulk (about 70%) of its rainfall in boreal summer from May to September (Fig. 2). As part of eastern China, the

variability of summer rainfall over NC is strongly modulated by the EASM (e.g., Zhao et al. 2010), which is linked to the conditions of Eurasian and Tibetan snows and tropical sea surface temperature (SST), among others (Yang and Xu 1994; Hu et al. 2003; Zhang et al. 2004; Wu et al. 2012b). On the interannual time scales, NC rainfall variability is partly caused by the large interannual variability of the EASM (e.g., Shi and Zhu 1996; Li et al. 2011a) and El Niño–Southern Oscillation (ENSO) (Dai and Wigley 2000; Guo et al. 2012). On interdecadal time scales, previous studies show that summer rainfall in NC has been decreasing since 1965; in particular, many studies have also revealed the prominent long-term change of summer rainfall over eastern China in the late 1970s (e.g., Weng et al. 1999; Ren et al. 2004; Xu 2001; Gong and Ho 2002; Zhou et al. 2006). Rainfall changes over East China have been characterized as a wetting trend over the middle-lower Yangtze River Valley (YRV) and a drying trend over the Yellow River valley during the past decades, a pattern referred to as ''southern flooding and northern drought'' in China (Yatagai and Yasunari 1994; Nitta and Hu 1996; Hu et al. 2003; Yu and Zhou 2007; Zhu et al. 2007). This pattern was further confirmed by the analyzing the long-term variations of the simulated summer climate over China (Hu et al. 2003). Interestingly, Zhao and Zhou (2006) showed that there is a ''negative–positive–negative'' tripole pattern in the interdecadal variability in summer rainfall over eastern China, with negative anomalies occurring over YRV and positive anomalies emerging over both southeastern and northern China. Ding et al. (2008) added that the interdecadal variability of summer rainfall over eastern China was characterized by two meridional modes: a dipole pattern and a positive–negative–positive pattern. As for the forcing of the interdecadal variability, previous studies suggested that the subtropical northwestern Pacific high and tropical Pacific SST play important roles in the rainfall variability over eastern China (Chang et al. 2000a,b). Additionally, Gong and Ho (2002) proposed that, since 1980, the variations of SST over the tropical Indian Ocean were primarily responsible for the shift of summer rainfall over eastern China through their effects on the subtropical northwestern Pacific high. Yang and Lau (2004) also showed a positive trend of summer rainfall over central-eastern China and a negative trend over northern China over the past 50 years and linked these trends to the interdecadal variations of global SST. In particular, the decadal variability of summer NC rainfall is strongly related to the decadal variation of the SLP over the southwest Indian Ocean and SST over the Indian–western Pacific warm pool (Guo et al. 2012).

Besides SSTs, summer rainfall changes over eastern China were also linked to the summer cooling at the upper troposphere over extratropical East Asia, which was assumed to be associated with stratosphere–troposphere interactions (Yu et al. 2004). Changes in both land temperature and SST that modified the land–ocean temperature gradient were also attributed to the southwesterly monsoon flow weakening and the moisture transport to southern China (Cheng et al. 2005). Moreover, rainfall changes in eastern China were also linked to increased aerosols from air pollution over East Asia (Menon et al. 2002; Qian et al. 2003; Cheng et al. 2005), the North Atlantic Oscillation (NAO) (Xin et al. 2006; Wu et al. 2009; Wu et al. 2012a), and the significant weakening of the tropical upper-level easterly jet (Yu et al. 2004; Ding et al. 2008). The effects of observed changes in SSTs, greenhouse gases, and aerosols during 1950–2000 on the EASM and rainfall changes are documented in the recent paper by Li et al. (2010). A systemic survey on the impacts of ocean–atmosphere interaction over the adjacent area of Asia and Indian–Pacific Ocean on EASM and summer rainfall over eastern China is given by Li et al. (2011a,b).

The above results suggest that rainfall in both NC and SWWA has declined since around the mid-1960s to 1970s: the reduction in rainfall over NC may be associated with the observed weakening EASM and other factors such as aerosols, SSTs, and the subtropical high anomalies in the western Pacific, while the decrease of SWWA winter rainfall may be attributed to a series of factors including natural variability, land-use changes, and atmospheric circulations over past decades. Apart from the long-term reduction of rainfall in both regions, monthly rainfall distribution shows that the bulk of rainfall in both NC and SWWA occurs from May to October (Fig. 2). It is known that the rainfall decrease in SWWA has only happened in early austral winter [May–July (MJJ)] (IOCI 2002; see our Figs. 3a–c), while the rainfall reduction in NC has decreased in late boreal summer [July–September (JAS); Figs. 3d–f]. As SWWA and NC regions are located at similar longitudes (i.e., about 111°–122°E) and latitudes (30°–35°S for SWWA and 36°–41°N for NC) in the Southern Hemisphere and Northern Hemisphere, respectively, it is suggestive to raise the question of whether there is a linkage between SWWA droughts caused by the reduction of SWWA MJJ rainfall and NC droughts induced by the decrease of NC JAS rainfall during 1951–2008, and what forcing drives such a teleconnection.

The purpose of this study is to investigate the teleconnection between the reduction of rainfall in SWWA and NC. Section 2 describes the datasets and methods used. Results concerning the rainfall teleconnection between SWWA MJJ rainfall and NC JAS rainfall are presented in section 3, and the possible driver of the teleconnection is discussed in section 4. A summary and discussion are given in section 5.

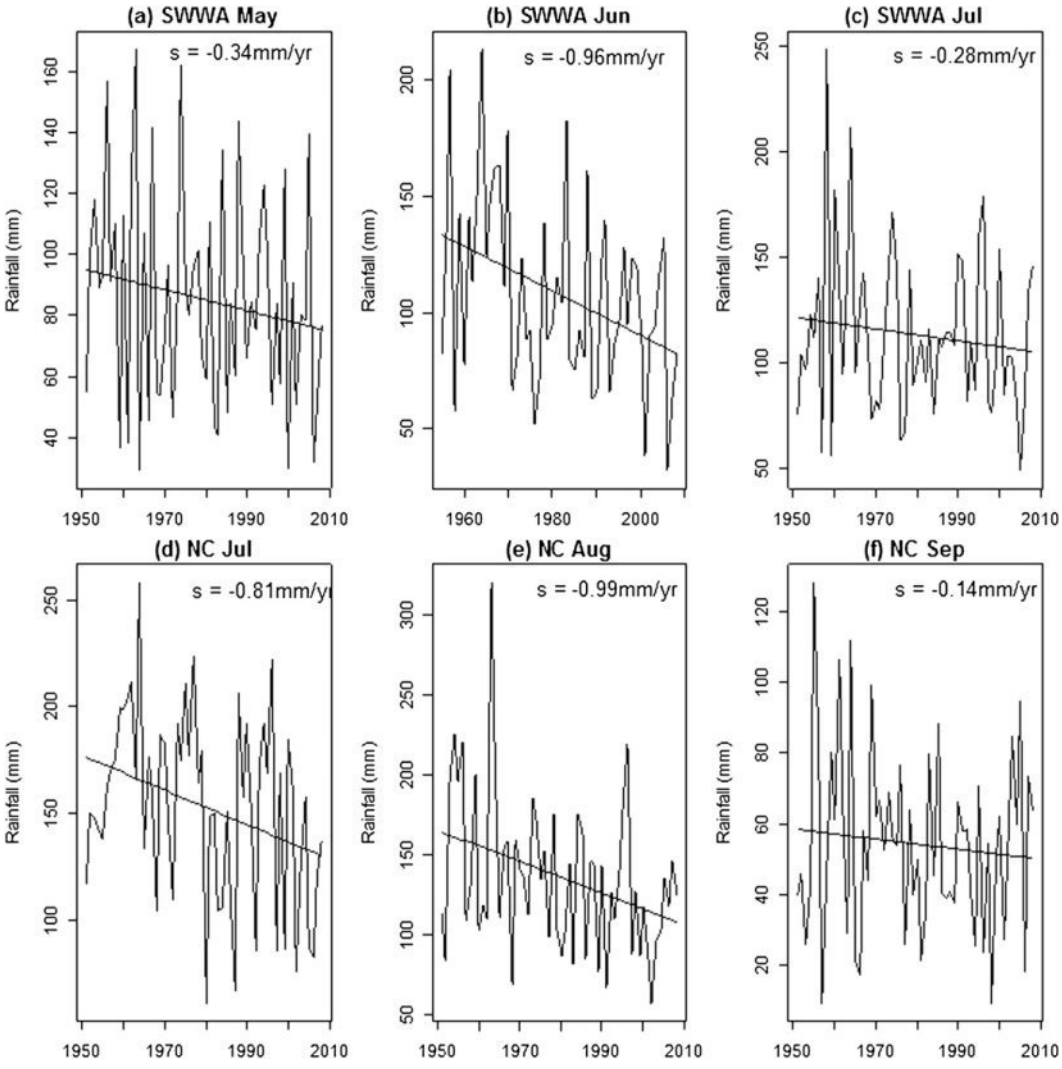

FIG. 3. (a)–(c) SWWA monthly 1951–2008 rainfall series and superimposed trend slopes for May–July; (d)–(f) As in (a)–(c), but for NC in July–September.

2. Data and methodology

a. Data

Sea level pressure, surface precipitable water (PWT), and winds at the 850-hPa level were extracted from the National Centers for Environmental Prediction (NCEP)–National Center for Atmospheric Research (NCAR) reanalysis globally archived dataset with a horizontal resolution of 2.5° × 2.5° (http://www.cdc.noaa.gov/index.html) (Kalnay et al. 1996). The SST data were taken from the Extended Reconstructed SST version 2 (ERSST V2) data (Smith and Reynolds 2004), which can be downloaded from the National Oceanic and Atmospheric Administration (NOAA) web site (http://www.esrl.noaa.gov/psd/data/gridded/data.noaa.ersst.html). The data analyzed here comprise the gridded MJJ and JAS average values for each year during the period from 1951 to 2008.

The ENSO index (Niño-3.4) was also downloaded from NOAA's website (http://www.esrl.noaa.gov/psd/data/climateindices/list/). The EASM, the NAO, and the SAM indices were downloaded from the web (http://ljp.lasg.ac.cn/dct/page/65544). The EASM index is defined as an area-averaged seasonally (JJA) dynamical normalized seasonality (DNS) at 850 hPa within the East Asian monsoon region (10°–40°N, 110°–140°E) (Li and Zeng 2002; Wang et al. 2008; Feng et al. 2010a; Li et al. 2012). The SAM index (SAMI) is defined as the difference in the normalized monthly zonal-mean sea level pressure between 40° and 70°S (Nan and Li 2003). This SAMI is a modification of the SAMI defined by Gong and Wang (1999), which is the difference in the normalized

TABLE 1. Station details and correlation with SWWA MJJ rainfall for individual NC station late summer (JAS) rainfall over 1951–2008 ($N = 58$). ''Station No.'' is the China Meteorological Administration identifier of each station. Stations listed here are ''high quality rainfall records'' from with the NC region. Correlation values are computed for the time series SWWA MJJ rainfall (r), its interannual component r_{IA} and interdecadal component (r_{ID}) obtained by using MODWD method. Statistical significance is shown with asterisks: $p < 0.1$ (a), $p < 0.05$ (b), $p < 0.01$ (c). The effective number of degrees of freedom (N^{eff}, N_{IA}^{eff}, and N_{ID}^{eff}) are calculated with account for autocorrelation in time series.

Station	Station No.	Lat (°N)	Lon (°E)	r	N^{eff}	r_{IA}	N_{IA}^{eff}	r_{ID}	N_{ID}^{eff}
Beijing	54511	39.93	116.28	0.19	41	−0.03	34	0.64[b]	7
Chende	54423	40.97	117.93	0.20[a]	41	0.00	29	0.71[c]	9
Zhangjiakou	54401	40.78	114.88	0.32[c]	56	0.27[b]	48	0.48[b]	12
Tianjin	54527	39.10	117.17	0.26[b]	45	0.18	33	0.55[b]	11
Shijiazhuang	53698	38.03	114.42	0.38[c]	56	0.27[b]	40	0.75[c]	11
Taiyuan	53772	37.78	112.55	0.22	47	0.10	33	0.69[c]	9
Xingtai	53798	37.07	114.50	0.27[b]	54	0.16	35	0.62[c]	13
Anyan	53898	36.12	114.37	0.28[b]	56	0.14	48	0.67[b]	9
Dezhou	54714	37.29	116.22	0.30[b]	53	0.17	41	0.65[c]	9
Weifang	54843	36.70	119.08	0.28[b]	48	0.21	34	0.48[a]	10
Qindao	54857	36.07	120.33	0.17	44	0.08	41	0.42	9
NC Ave	...	...	...	0.43[c]	43	0.26[a]	38	0.82[c]	7

zonal-mean SLP between 40° and 65°S (available from http://ljp.lasg.ac.cn/dct/page/65544). The Indian Ocean dipole (IOD) index (IODI; Saji et al. 1999) is downloaded from the Japan Agency for Marine-Earth Science and Technology (JAMSTEC; http://www.jamstec.go.jp/frcgc/research/d1/iod/).

The rainfall data in Australia analyzed here were provided by the National Climate Centre (NCC) of the Bureau of Meteorology (BoM) and consist of gridded data on a 0.25° × 0.25° grid. These are described by Lo et al. (2007), who indicate their confidence in the validity of the data over after 1948. In addition, SWWA was selected as the region southwest of the line joining 30°S, 115°E and 35°S, 120°E (Fig. 1). Time series of SWWA MJJ rainfall totals ($SWWAR_{MJJ}$) over the 58-yr period from 1951 to 2008 are generated (from the BoM web site http://www.bom.gov.au/cgi-bin/silo/cli_var/area_timeseries.pl).

Rainfall data in China used here are monthly station rainfall data at 160 stations in China provided by the Chinese Meteorological Administration (CMA). These station observations are operated by the CMA consistently through the observation period, meeting the standards of the World Meteorological Organization. North China (NC) refers to the region bounded by 36°–41°N and 111°–122°E with the right-hand side boundary being the coastline (see box in Fig. 1). The NC averaged rainfall total (NCR_{JAS}) series were calculated based the 11 stations including Beijing, Tianjin, Shanxi, Shandong, and Hebei municipalities or provinces (Table 1).

b. Methodology

Rainfall in both the SWWA and NC regions has strong interannual and interdecadal variabilities. To see if the SWWA–NC rainfall relation holds at interannual and decadal time scales, we apply a wavelet method based on the maximal overlap discrete wavelet transform (MODWT; Percival and Mofjeld 1997) to decompose rainfall series into different subseries with various frequencies (i.e., interannual and interdecadal variability). The MODWT of a time series leads to an additive decomposition known as multiresolution analysis, which breaks up the series into a number of ''details'' and a single ''smooth.'' Each detail is a time series describing variations at a particular time scale, whereas the smooth describes the low-frequency variations. Mathematically, suppose that a time series $\mathbf{X}_t = \{X_t: 1 \le t \le N\}$ was collected at time $t\Delta t$, where Δt is the time interval between the adjacent observations (e.g., $\Delta t = 1$ yr for $SWWAR_{MJJ}$ and NCR_{JAS}). Then original time series $\{\mathbf{X}_t, 1 \le t \le N\}$ can be decomposed into detail and smooth components as follows:

$$\mathbf{X}_t = \sum_{j=1}^{J} D_j(t) + S_J(t), \tag{1}$$

where details $D_j = D_j(t)$, an N-dimensional column vector whose elements are associated with changes at the time scale $2^j\Delta t$, $j = 1, \ldots, J$, and the smooth $S_J = S(t)$, which is a similar vector with elements associated with variations at scales of $2^{J+1}\Delta t$ and higher. The D_j and S_J series are associated with the zero phase filters, making it possible to line up features in a multiresolution analysis with the original time series. More information on implementing MODWT may be found in appendix A.

We will focus on investigating the relationship between time series of $SWWAR_{MJJ}$ and NCR_{JAS} at interannual and interdecadal time scales using the decomposed rainfall series by MODWT. The interannual component

is represented by the sum of details (D1 + D2) associated variations at 2–7 years, and the decadal to interdecadal component by the smooth S2 with variations longer than 8 years, respectively. Hereafter, we use ''interdecadal'' to denote the ''decadal to interdecadal'' without a distinction.

Because the decomposed rainfall series ($SWWAR_{MJJ}$ and NCR_{JAS}) are serially autocorrelated on interdecadal time scale, to test the significance of correlation between them we have adjusted degrees of freedom (df) using an effective number of degree of freedom estimated by the modified Chelton method (Pyper and Peterman 1998). See appendix B for more details about testing the significance of the correlation between two autocorrelated time series using this method.

3. Linking SWWA to NC climate

a. Rainfall teleconnection

As stated in the introduction, we know that rainfall in both SWWA and NC has been declining substantially since the mid-1960s. Indeed, a more detailed study on trends in monthly rainfall in both SWWA and NC regions indicates that the decline of rainfall in SWWA only happens in early austral winter (May–July; Figs. 3a–c), whereas rainfall reduction in NC occurs in late boreal summer (July–September; Figs. 3d–f). So we focus on decreasing trends in $SWWAR_{MJJ}$ and NCR_{JAS}.

Figures 4a and 4c show the rainfall trend map over Western Australia in MJJ and eastern China in JAS, respectively. There is an almost coherent decreasing trend in rainfall over Western Australia in MJJ, with the strongest decreasing trends in the SWWA region (Fig. 4a). On the other hand, there is a clear dipole structure (''southern wet and northern dry'') in the observed rainfall trend over eastern China in JAS: rainfall is increasing in southeast of eastern China, whereas rainfall tends to decrease in southwest, central, and north-northeast China with the strongest decreasing trend located in the region of NC and central west of eastern China (Fig. 4c). The rainfall at the southeast coast stations does not show a significant decreasing tendency, which may be partly due to the southward shift of the subtropical jet (Li et al. 2010) and partly to the strengthened linkage with ENSO (Wu et al. 2012b). As a result, $SWWAR_{MJJ}$ has a drying trend of -1.53 mm yr^{-1} and NCR_{JAS} experiences a stronger decreasing trend of -1.95 mm yr^{-1}, both significant at the 0.01 level (Figs. 4b,d). Besides the long-term drying trend in both regions, there is also similar interdecadal variability in $SWWAR_{MJJ}$ and NCR_{JAS} (i.e., the smooth curves in Figs. 4b and 4d). In particular, there is a link between the raw time series of $SWWAR_{MJJ}$ and NCR_{JAS} in 1951–2008, with a correlation of 0.43, significant at the 0.01 level. This link remains after the data are detrended, with a correlation of 0.33, significant at the 0.05 level.

Figure 5 shows the decomposed interannual and decadal time series of $SWWAR_{MJJ}$ and NCR_{JAS} using the MODWT technique. On the interannual time scale, $SWWAR_{MJJ}$ has a link to NCR_{JAS} with a correlation of 0.26 (significant at 0.10 level with an effective sample size $N_{IA}^{eff} = 38$), and the linkage on the interdecadal time scale becomes highly significant at the 0.01 level with $N_{ID}^{eff} = 7$ and a correlation of 0.82 (cf. Figs. 5e and 5f). Here N_{IA}^{eff} and N_{ID}^{eff} denote the effective degree of freedom by adjusting the degree of freedom for interannual (D1 + D2) and decadal (S2) time series of $SWWAR_{MJJ}$ and NCR_{JAS}. Because of the highly significant correlation between $SWWAR_{MJJ}$ and NCR_{JAS} on the interdecadal time scales, rainfall in both SWWA and NC has experienced a similar interdecadal variability: a wetting period during 1950 to the mid-1960s, a shift from low to high about 1980, and a shift from high to low rainfall around 1992 (Figs. 5e,f).

As shown in Table 1 and Fig. 6, for individual stations, a general pattern at decadal time scales emerges with stronger correlations (reaching $r = 0.75$, significant at the 0.01 level at Shijiazhuang) for stations in the west, center, and east NC, diminishing to south and the southeast. Indeed, two stations located at the southeast coast (Qindao and Weifang) show no significant correlation with SWWA. The southeast coast stations showing weak relationships to the SWWA region is consistent with local rainfall associated with northward flow and the dipole structure of China rainfall: southern flooding and northern drought.

Regional patterns are more clear from comparison to the correlation map between $SWWAR_{MJJ}$ (NCR_{JAS}) and JAS rainfall over eastern China (MJJ rainfall over Western Australia) using grid rainfall data (Fig. 7). On the interdecadal time scale, the readily apparent patterns are that the $SWWAR_{MJJ}$ has a significant correlation with JAS rainfall confined to the northeast of China including the NC region (Fig. 7a), while the NCR_{JAS} has a strong correlation with MJJ rainfall in a large part of southwest Western Australia beyond the SWWA region (Fig. 7b). However, there is only weak signal of the correlations on the interannual time scale: $SWWAR_{MJJ}$ has a silent correlation with NCR_{JAS} (Fig. 7c), although NCR_{JAS} does show significant correlations at the 0.05 level with $SWWAR_{MJJ}$.

Taken together, the evidence suggests a statistically significant link between $SWWAR_{MJJ}$ and NCR_{JAS}. The link is stronger on interdecadal time scales, but weaker on the interannual time scale. This result is consistent

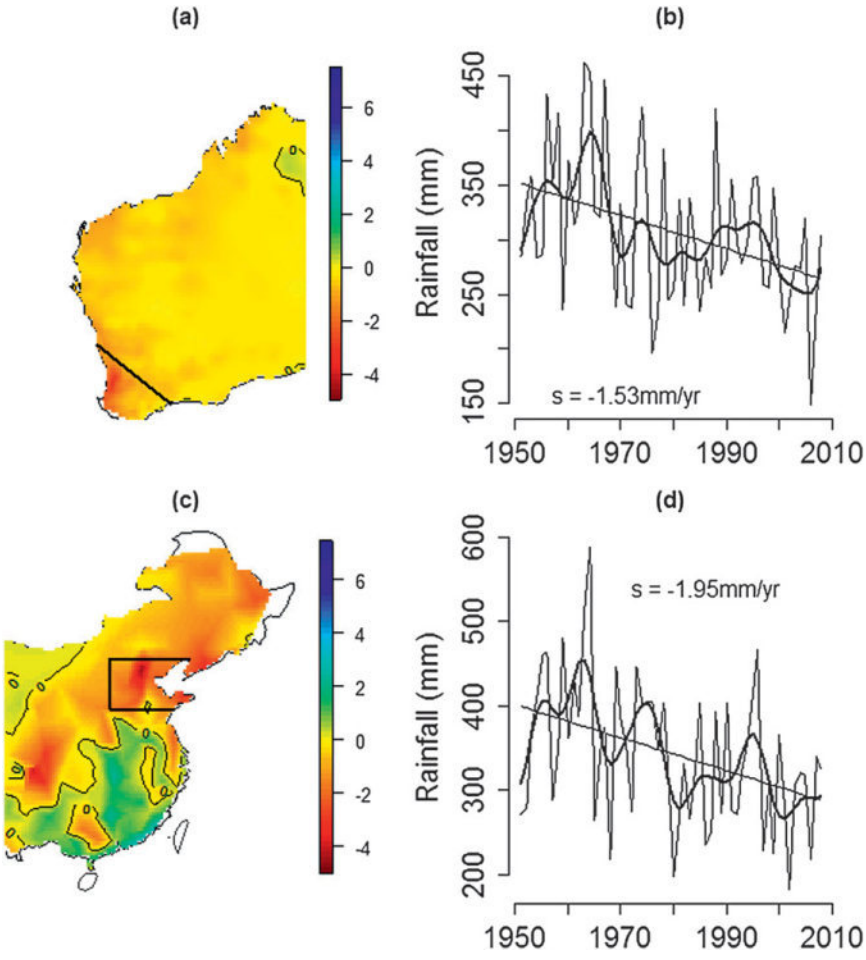

FIG. 4. (a) Spatial pattern of trend (mm yr^{-1}) in MJJ total rainfall over Western Australia during 1951–2008. (b) Time series of $SWWAR_{MJJ}$ and its superimposed trend (-1.53 mm yr^{-1}). (c) Spatial pattern of trend (mm yr^{-1}) in JAS total rainfall over East China during 1951–2008. (d) Time series of NCR_{JAS} rainfall and its superimposed trend (-1.95 mm yr^{-1}) over the period 1951–2008. The smooth curves in (b) and (d) are the estimated $SWWAR_{MJJ}$ and NCR_{JAS} interdecadal components; The black lines are drying trends in both regions, which are highly significant at the 0.01 level.

with the fact that smoothing acts to reduce transient meteorological noise superimposed on the large-scale circulation modes, which drive the teleconnection, thus increasing the observed correlation (van Ommen and Morgan 2010). It also indicates that the mechanisms driving the linkage between $SWWAR_{MJJ}$ and NCR_{JAS} are different at interannual and interdecadal time scales.

b. *Atmospheric links*

Figure 8a shows the correlation of $SWWAR_{MJJ}$ with MJJ SLP over the large area bounded by 60°N–60°S and 80°–160°E. The high rainfall is accompanied by low pressures over most of the Australian region, with the strongest correlations (exceeding -0.8) over the southwest. This is expected given that the relationship that $SWWAR_{MJJ}$ is well coupled with a regional circulation over wider southwest Australia, which is highly associated with SWAC (Feng et al. 2010a). What is unexpected is that the significant inverse relationship with MJJ SLP crossed the equator and formed a cyclone pattern centered in East Asia (30°–50°N, 100°–115°E) (Fig. 8a), with an associated positive relationship with the PWT over NC (Fig. 8c). In particular, the inverse relationship is more pronounced between $SWWAR_{MJJ}$ and JAS SLP over NC (Fig. 8b), and so is the positive relationship between $SWWAR_{MJJ}$ and JAS PWT over NC (Fig. 8d). Therefore, the high $SWWAR_{MJJ}$ value is expected to be significantly correlated with low pressure and high PWT in JAS over NC, which favor to high rainfall over NC.

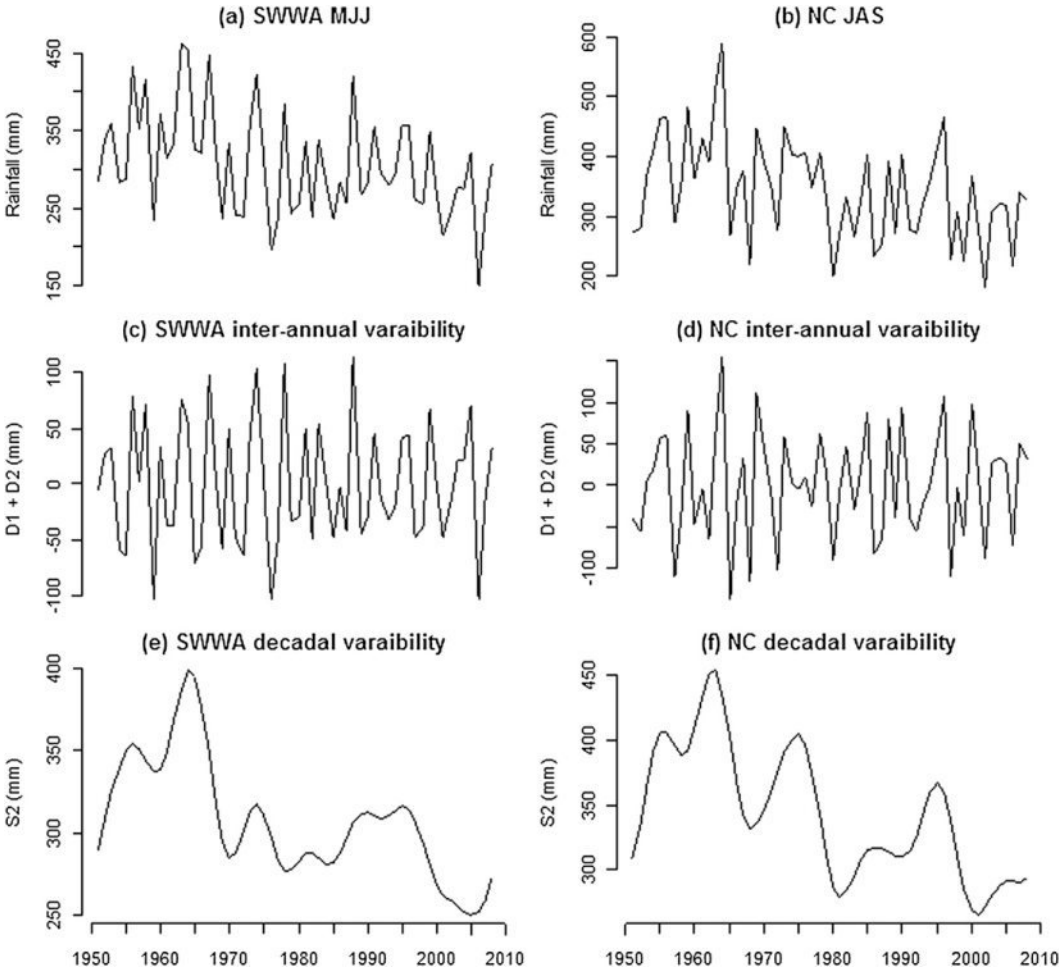

FIG. 5. (a) SWWA MJJ rainfall over 1951–2008. (b) As in (a), but for NC JAS rainfall. (c) The interannual variability of SWWA MJJ rainfall. (d) As in (c), but for NC JAS rainfall. (e) The interdecadal variability of SWWA MJJ rainfall. (f) As in (d), but for NC JAS rainfall. The interannual variability is defined as the sum of details (D1 + D2) and the interdecadal variability as the smooth component (S2) by MODWT multiresolution analysis based on the LA(8) wavelet filter. Details D_1, D_2 and smooth S_2 series have respective frequencies of 2–4 yr, 4–8 yr, and <8 yr.

To further understand the atmospheric links associated with the connection between $SWWAR_{MJJ}$ and NCR_{JAS}, we constructed two composite fields for 850-hPa geopotential height (HGT850) and winds for the difference when both $SWWAR_{MJJ}$ and NCR_{JAS} are in dry years (i.e., 1972, 1980, 1987, 1989, 1997, 2001, 2002, and 2006, when rainfall is lower than the mean minus half standard deviation) and wet years (i.e., 1956, 1963, 1964, 1973, 1974, 1978, 1988, 1995, and 1996, when rainfall is higher than the mean plus half standard deviation) during the 1958–2008 period (Figs. 9a,b). Note that these selected years with high and low rainfall in both NC and SWWA reflect an interdecadal feature characterized by more wet (6 out of 9) years before 1980 and more (7 out of 8) dry years after 1980. This feature is consistent with results from many studies that NC and SWWA rainfall have decreased since late 1970s. Additionally, the composite results of 850-hPa winds and geopotential height fields are consistent with the observations from the correlation map in Figs. 8a and 8b. In MJJ, the composite of HGT850 difference shows two anomalous anticyclone patterns: one is close to the SWWA region and the other is in East Asia centered near 35°–50°N, 100°–115°E. The anomalous anticyclone near SWWA and associated easterlies leads the lower rainfall in SWWA while the northern anticyclone associated with north–south wind over NC region will suppress rainfall in this region (Fig. 9a). Another striking feature is that, while the anticyclone near SWWA was weakening in JAS, the northern anticyclone was persistent into JAS and became stronger, leading to anomalous strong northeasterlies crossing the NC, implying rainfall reduction (Fig. 9b). Therefore, atmospheric

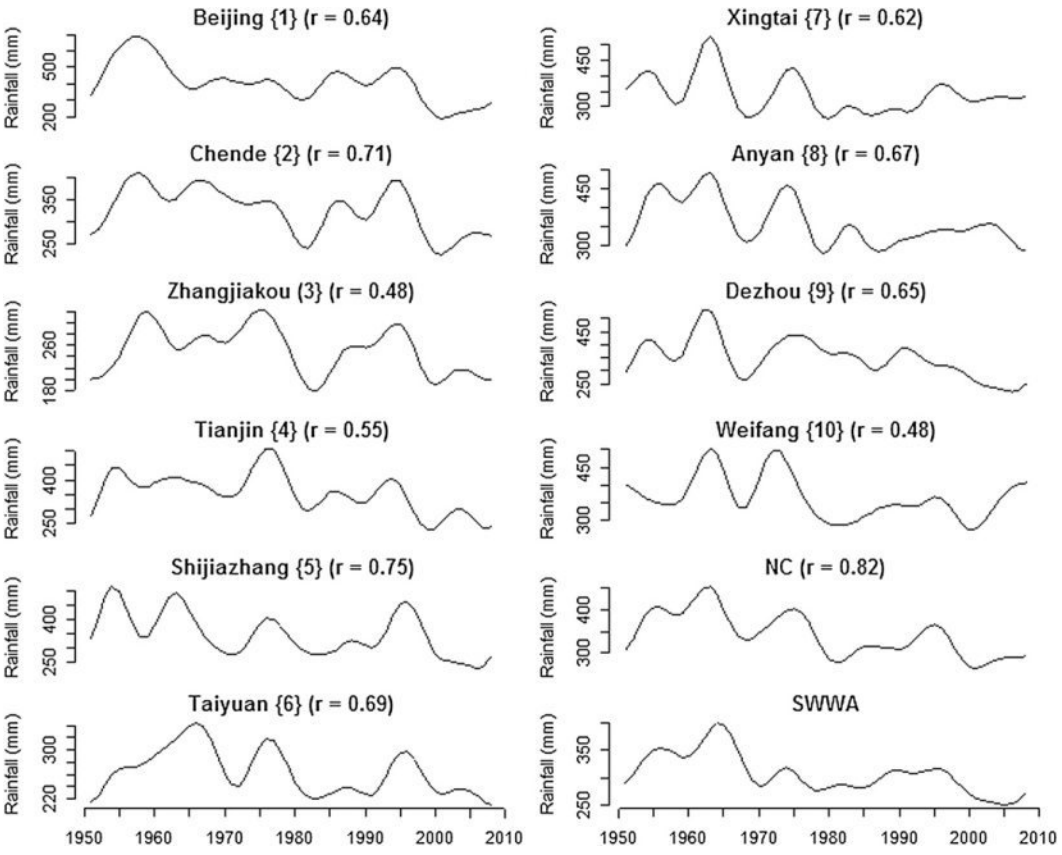

FIG. 6. Time series and correlation for SWWA MJJ and NC JAS rainfall at 11 stations over NC at interdecadal time scales during 1951–2008.

circulations leading to a teleconnection between $SWWAR_{MJJ}$ and NCR_{JAS} may be due to two anticyclone systems in the Southern and Northern Hemispheres. The southern anticyclone is weakening from MJJ to JAS, while the northern anticyclone is persistent to JAS and becomes stronger, which implies a significant correlation relationship between $SWWAR_{MJJ}$ and NCR_{JAS}. We will come back to this point in the next section on drivers associated with this relationship.

4. Possible drivers of the teleconnection

The above analysis suggests a statistically significant link between $SWWAR_{MJJ}$ and NCR_{JAS} (Figs. 5–7; Table 1) through two anticyclones close to the SWWA region and East Asia centered near 35°–50°N, 100°–115°E (Figs. 8, 9). This teleconnection manifests significantly at interdecadal time scales but is weak on the interannual time scale. Accordingly, we investigate in this section the driving force of the teleconnection between $SWWAR_{MJJ}$ and NCR_{JAS} on decadal time scales.

Previous study shows that neither the tropical Indo-Pacific phenomena (ENSO, the IOD, and ENSO-Modoki) nor the SAM has a consistent role to play in the variability of SWWA rainfall because they decoupled from the rainfall during either 1948–78 or 1979–2006 (see Table 1 in Feng et al. 2010b). Hence they cannot cause the trend in early winter rainfall over SWWA in the past decades. On the other hand, Feng et al. (2010a) suggest that a monsoon-*like* southwest Australia circulation may contribute to the rainfall decline in early winter (May–July) over SWWA. They found that the MJJ SWAC can explain not only the interannual variability of the SWWA MJJ rainfall but also the long-term decreasing trend in the SWWA MJJ rainfall. The driver of the SWAC may be the shift of the planetary-scale thermal convection (Zeng and Li 2002), associated with the shift of the subtropical high resulted in the reversal winds over SWWA, which may be linked to the poleward expansion of the Hadley circulation and the subtropical dry zone (Lu et al. 2007). Moreover, the summer rainfall reduction in NC has been related to the subtropical high anomalies in the western Pacific (Zhang 1999). These known results motivate us to investigate whether the teleconnection between $SWWAR_{MJJ}$ and NCR_{JAS} is driven by the poleward shifts of both southern and northern subtropical ridges

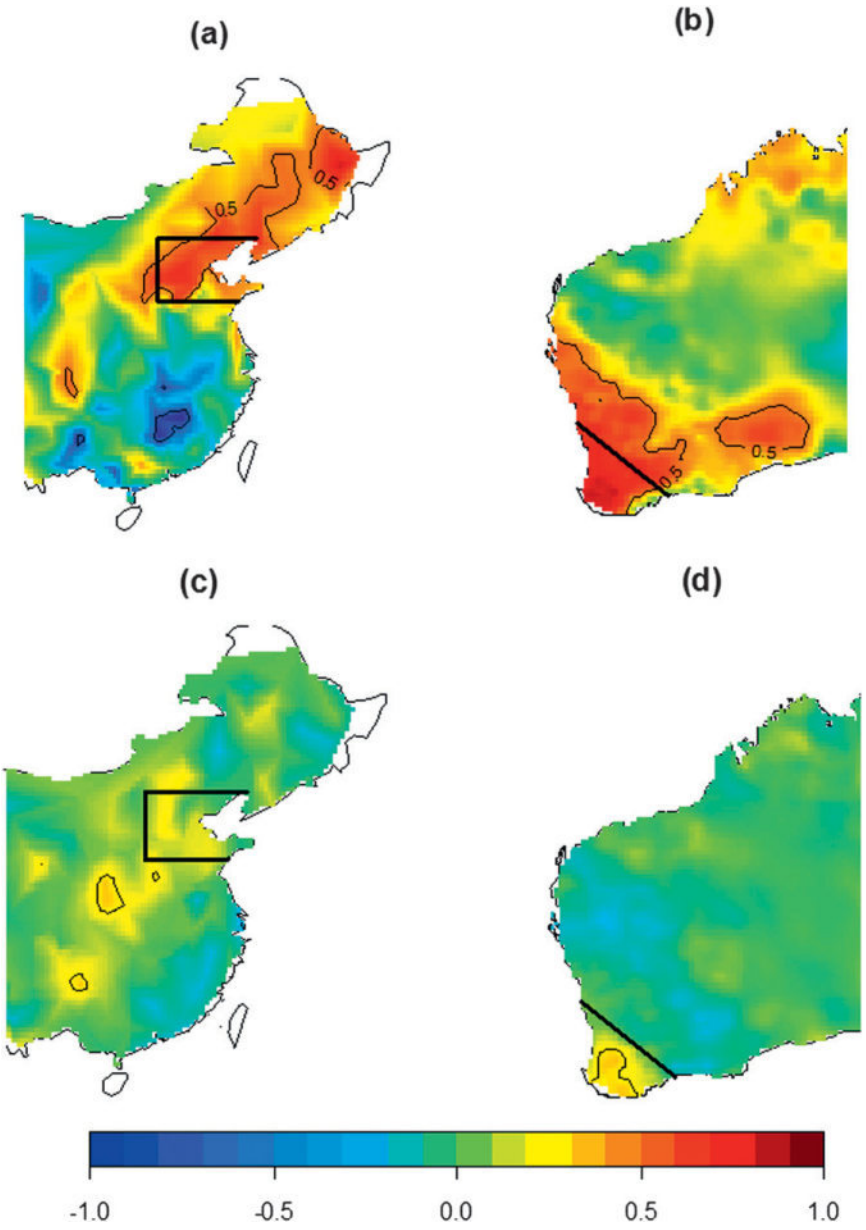

FIG. 7. (a) Spatial pattern of interdecadal correlations between $SWWAR_{MJJ}$ and rainfall over eastern China in JAS during 1951–2008. (b) Spatial pattern of interdecadal correlations between NCR_{JAS} and rainfall over Western Australia in JAS during 1951–2008. (c) As in (a), but on an interannual time scale. (d) As in (b), but on interannual time scale. The correlations significant at 0.1 levels (0.5 for interdecadal and 0.26 for internal time scales) are marked in contour lines.

caused by the poleward expansion of the Hadley circulation and the subtropical dry zones in both hemispheres.

Figure 10 shows the time–latitude section of the mean position of the subtropical high ridge over 110°–150°E at 925 hPa for MJJ and JAS in the Southern Hemisphere (Figs. 10a,b) and Northern Hemisphere (Figs. 10c,d). In MJJ from 1948 to 2008, the averaged position of the southern subtropical high ridge (SSHR) bears a significant southward trend (Fig. 10a) while there is a nonsignificant weak upward trend in JAS. It is known that the position of the SSHR is significantly correlated with the SWAC index at the 0.01 level, with a correlation coefficient of 0.89 in MJJ and 0.84 in JAS, and there is a well-coupled SWAC–SWWA rainfall relation (Feng et al.

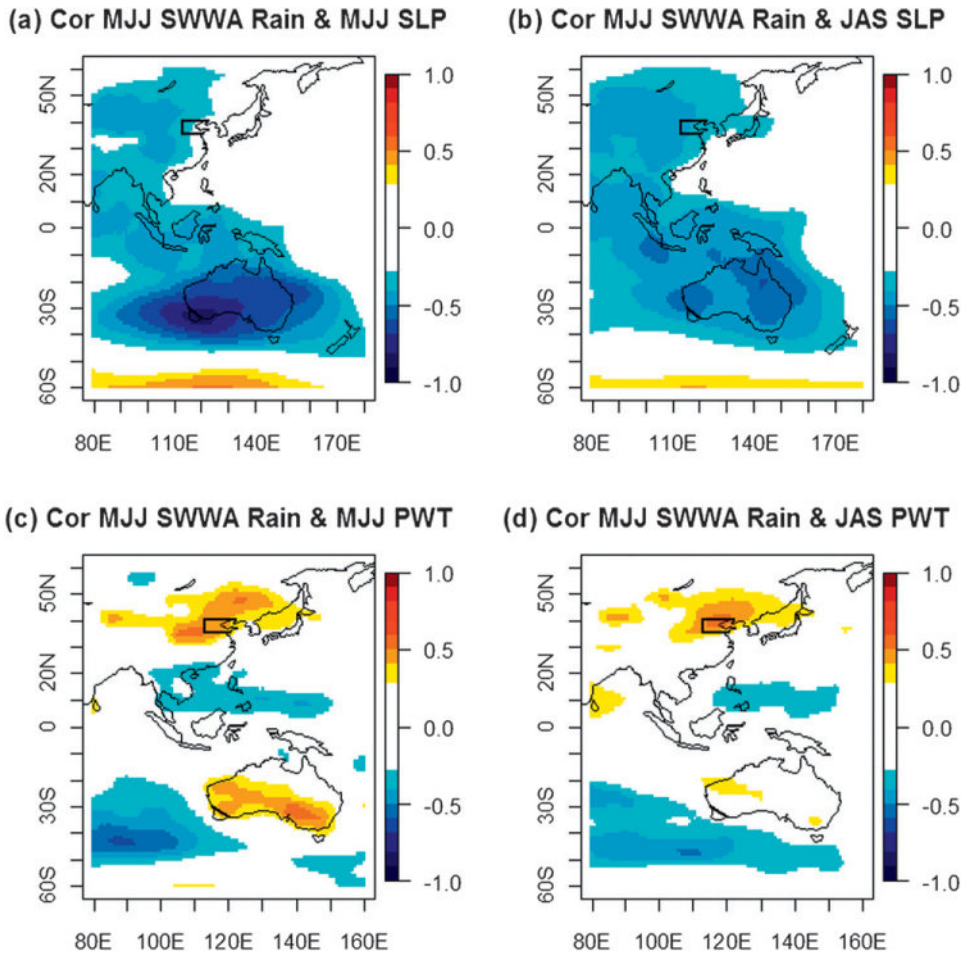

FIG. 8. Correlation map for the MJJ rainfall series averaged over SWWA with NCEP sea level pressure in (a) MJJ and (b) JAS, and with NCEP surface precipitable water (PWT) in (c) MJJ and (d) JAS. Only significant correlations at the 0.05 level are plotted and marked in colors. Each contour level is 0.1.

2010a). Thus, the poleward shift of the SSHR may cause the weak SWAC and less rainfall over SWWA in MJJ, while the nonsignificant weak upward trend in position of the SSHR in JAS implies a slight increase in the strength of the SWAC and rainfall over SWWA (IOCI 2002). Indeed, the significant poleward shift of the MJJ SSHR may induce an anomalous anticyclone centered below the south Australian coast, which leads to the anomalous easterlies causing the reduction of $SWWAR_{MJJ}$, as shown in the 925-hPa wind and height anomaly composite constructed by computing the difference between strong and weak poleward years of the SSHR (Fig. 10e). Here a strong (weaker) poleward year of the SSHR is defined as a year with its position higher (lower) than one standard devotion of the averaged position of the SSHR over 1948–2008. In contrast, the northern subtropical high ridge (NSHR) shows a weak poleward shift in MJJ (Fig. 10c) but a significant poleward shift trend in JAS from 1948 to 2008 (Fig. 10d). The significant poleward shift of the NSHR in JAS indicates more anticyclones centered over northwest NC, which leads to the anomalous northerlies resulting in less water vapor to NC, and the reduction of late summer rainfall in NC, as shown in the 925-hPa water vapor and geopotential height anomaly composite associated with the difference between strong and weak poleward years of the NSHR (Fig. 10f). Therefore, the poleward shift of the SSHR–NSHR can pinned down the mechanism of behaviors of the southern anticyclone cannot be persistent to JAS, while the northern anticyclone is persistent to JAS and became stronger. That is, associated with strong poleward shift of the SSHR in MJJ (Fig. 10a), the southern anticyclone is strong in MJJ (Fig. 10e), but it cannot persist to JAS (not shown) because of the lack of the poleward shift of the SSHR in JAS (Fig. 10b); similarly, associated with the weak poleward shift of the NSHR in

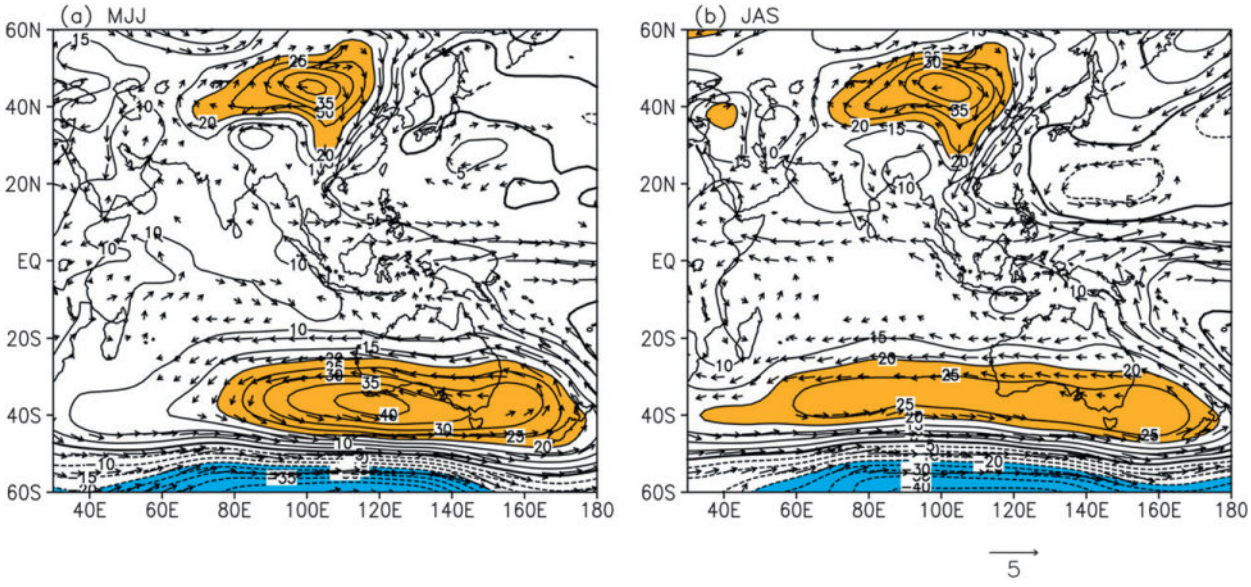

FIG. 9. (a) Composite difference (dry minus wet years) of MJJ 850-hPa winds (m s^{-1}) and geopotential height (gpm) when both SWWA MJJ and NC JAS rainfall are lower and higher during 1951–2008. (b) As in (a), but for the composite difference of JAS. Vector winds are plotted where they are deemed to significantly differ from 0 at the 0.10 level based on a *t* test. Positive (negative) contours of geopotential height > 20 gpm (< -20 gpm) are marked in yellow (blue).

MJJ (Fig. 10c), a weaker northern anticyclone appears near NC in MJJ (not shown), and persistently becomes strong in JAS (Fig. 10f) because of the strong poleward shift of the NSHR in JAS (Fig. 10d).

The above results further suggest that the poleward shifts of SSHR and NSHR may lead to the teleconnection between $SWWAR_{MJJ}$ and NCR_{JAS}. As shown in Table 2, the teleconnection between $SWWAR_{MJJ}$ and NCR_{JAS} via the SSHR and the NSHR can be further demonstrated by the facts that 1) there is a highly significant correlation 0.82 between $SWWAR_{MJJ}$ and NCR_{JAS}; 2) the SSHR in MJJ ($SSHR_{MJJ}$) has a close link to the NSHR in JAS ($NSHR_{JAS}$), with a correlation of -0.51, significant at the 0.10 level; and 3) the relationship between $SWWAR_{MJJ}$ and NCR_{JAS} becomes not significant, with a correlation of 0.17, after removing the effect of the $SSHR_{MJJ}$ on $SWWAR_{MJJ}$ and the influence of the $NSHR_{JAS}$ on NCR_{JAS}. Therefore, the poleward shifts of SSHR and NSHR may lead to the teleconnection between $SWWAR_{MJJ}$ and NCR_{JAS}. This also raises a question about what drives the poleward shifts of the SSHR and the NSHR. Is there a common forcing driving the physical processes associated with the poleward shifts of the SSHR and the NSHR?

Figure 11a shows the Indian–Pacific SST anomalies associated with the $SSHR_{MJJ}$. It can be seen that significant correlations between the $SSHR_{MJJ}$ and SSTs exist in the Indian Ocean and western Pacific, as well as in sporadic regions over eastern Pacific. A similar pattern is also evident between the $NSHR_{JAS}$ and SSTs in the Indian Ocean and western Pacific (Fig. 11d). These results indicate that the warming SSTs in the tropical Indian–western Pacific (TIWP; 10°N–10°S, 60°–130°E) may have played a role in causing the poleward shift of the $SSHR_{MJJ}$. To confirm this, we calculated partial correlation between the $SSHR_{MJJ}$ and SSTs by linearly removing the effect of TIWP index (TIWPI; averaged SSTs over the region bounded by 10°N–10°S, 60°–130°E). As expected, significant correlations between the $SSHR_{MJJ}$ and SSTs virtually disappear after removing the effect of TIWPI in MJJ (Fig. 11b). Therefore, the poleward shift of the $SSHR_{MJJ}$ (Figs. 10a and 11c) is instigated by the warming SSTs in the TIWP region. Similarly, the poleward shift of the NSHR in JAS ($NSHR_{JAS}$) is largely due to the warming SSTs in JAS over the TIWP region ($TIWP_{JAS}$) (Figs. 11d–f). Note that the significant positive (and negative) correlations between the $NSHR_{JAS}$ and SSTs remain over the west subtropical Indian Ocean (and off the northwest Western Australian coast), implying that some other forcing (e.g., the IOD) may also contribute to the poleward shift of the $NSHR_{JAS}$. Indeed, as shown in Table 2, the IOD in JAS (IOD_{JAS}) has a close relation with the $NSHR_{JAS}$, with a correlation 0.62 significant at 0.05 level. However, the correlation between the $NSHR_{JAS}$ and the IOD_{JAS} becomes 0.33, not significant after removing the effect of the $TIWP_{JAS}$. Therefore, the warming SSTs in the TIWP region (i.e.,$TIWP_{JAS}$) have the dominant influence on the poleward shift of the $NSHR_{JAS}$ as shown in Fig. 11.

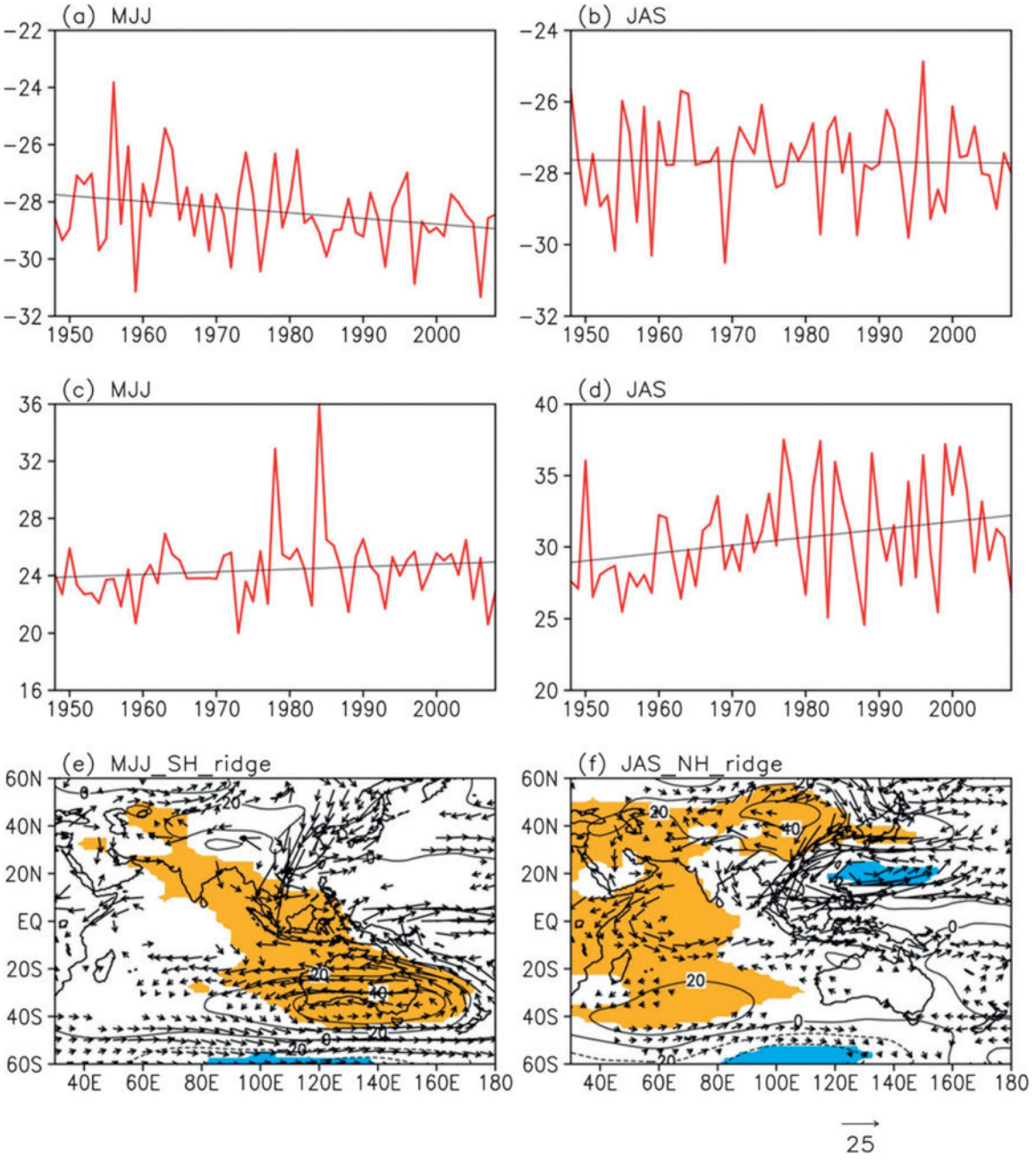

FIG. 10. Time–latitude section of the mean position of the (a),(b) SSHR and (c),(d) NSHR over 110°–150°E at 925 hPa in (left) MJJ and (right) JAS. Note that trends in (a) and (d) are significant at 0.05 level. (e),(f) The composite difference of anomalies between strong and weak poleward years of the SSHR in MJJ and NSHR in JAS, respectively. Only significant anomalies at the 0.05 level of geopotential height (contour lines) and water vapor transport at 925 hPa (vectors) are plotted.

In summary, on the interdecadal time scale, there is a highly significant teleconnection between $SWWAR_{MJJ}$ and NCR_{JAS}. The teleconnection is through the poleward shift of the $SSHR_{MJJ}$ and $NSHR_{JAS}$, which can be attributed the common forcing of the warming SSTs over the TIWP by observing that the averaged MJJ SSTs over the tropical Indian–western Pacific have a strong correlation (0.98) to the averaged JAS SSTs over the tropical Indian–western Pacific.

5. Conclusions and discussion

In this work, the teleconnection between $SWWAR_{MJJ}$ and NCR_{JAS} is studied. It is found that in early austral

TABLE 2. Correlations of $SWWAR_{MJJ}$ and NCR_{JAS} with other variables on the interdecadal time scales during 1951–2008. Here "$X \mid Y$" means the residuals of X after linear removing the effect of Y, where X and Y denote any variables listed in the table. Statistical significance is shown with asterisks: $p < 0.1$ (a), $p < 0.05$ (b), $p < 0.01$ (c).

	NCR_{JAS}	$NCR_{JAS} \mid NSHR_{JAS}$	$NSHR_{JAS}$	$SSHR_{MJJ}$	$NSHR_{JAS} \mid TIWP_{JAS}$
$SWWAR_{MJJ}$	0.82[c]	0.40	0.62[b]	0.77[c]	0.41
$SWWAR_{MJJ} \mid SSHR_{MJJ}$	0.44	0.17	−0.45	−0.03	−0.35
$SSHR_{MJJ}$	0.63[b]	0	−0.51[a]	1	−0.01
$SSHR_{MJJ} \mid TIWP_{MJJ}$	0.14	0.14	0	0.7	−0.06
$EASM_{JAS}$	0.38	0.40	−0.13	0.33	0.07
IOD_{JAS}	−0.41	−0.04	0.62[b]	−0.43	0.33
$Nino3.4_{JAS}$	−0.44	−0.33	0.29	−0.23	−0.01
NAO_{JAS}	−0.17	−0.23	0.01	0.02	0.01
SAM_{JAS}	−0.57[a]	−0.40	0.41	−0.75[b]	0.06

winter, the poleward shift of the SSHR in the past decades can induce an anomalous anticyclone centered near the south Australian coast, which leads to the anomalous easterlies causing the reduction of MJJ rainfall in SWWA. Similarly, the intensified poleward shift of the NSHR in the Northern Hemisphere can lead to an anticyclone centered over northwest of NC, which causes the anomalous northerlies resulting in the reduction of late summer rainfall in NC. The poleward shift of the $SSHR_{MJJ}$ and $NSHR_{JAS}$ can be attributed to the common forcing of the warming SSTs over the TIWP. Therefore, our results suggest that the poleward shifts of the SSHR and the NSHR instigated by the warming SSTs in the TIWP may have partially attributed to the rainfall reduction in both regions. They provide a strong support to the argument that the poleward expansion of the Hadley circulation and the subtropical dry zone may have influenced the climate in subtropical and extra-subtropical regions. To justify this argument, we need to discuss the influence of the well-known climate drivers (such as ENSO, the EASM, the IOD, the NAO, and the SAM) on the teleconnection between $SWWAR_{MJJ}$ and NCR_{JAS}.

The poleward shift of the $SSHR_{MJJ}$ and the $NSHR_{JAS}$ is largely independent of well-known phenomena such as ENSO, the EASM, and the NAO because there is no significant correlation between the $SSHR_{MJJ}$ ($NSHR_{JAS}$) and these climate drivers on interdecadal time scales (Table 2). The teleconnection between $SWWAR_{MJJ}$ and NCR_{JAS} is not influenced by linearly removing the influence of ENSO, the EASM, and the NAO, respectively. This can be demonstrated by the fact that the partial correlations between time series $SWWAR_{MJJ}$ and NCR_{JAS} are same as the raw correlation (0.82) after removing the EASM and the NAO indices in MJJ and JAS, and are slightly decreased to 0.75 and 0.80 when the effect of ENSO (i.e., Niño-3.4) is removed in MJJ and JAS. It is worth noting that the EASM has only a weak link (correlation = −0.13) with the $NSHR_{JAS}$ on interdecadal time scales; in contrast with the well-established fact that the NSHR (also known as the western Pacific subtropical high) is a principal component of the EASM system in late summer on interannual time scales (Wang et al. 2009).

We have demonstrated that the IOD_{JAS} has a close relation with the $NSHR_{JAS}$, yet the relationship between the $NSHR_{JAS}$ and the IOD_{JAS} becomes not significant after removing the effect of the $TIWP_{JAS}$. This indicates that the $TIWP_{JAS}$ has the dominant influence on the poleward shift of the $NSHR_{JAS}$. The secondary role of the IOD can be also demonstrated by its little influence on the teleconnection between $SWWAR_{MJJ}$ and NCR_{JAS}; that is, the partial correlation between time series $SWWAR_{MJJ}$ and NCR_{JAS} is slightly decreased to 0.78 by removing the IOD effect in MJJ and JAS.

On interdecadal time scales, the SAM has strong links with $SWWAR_{MJJ}$ (correlation = −0.81) and NCR_{JAS} (correlation = −0.57). The teleconnection between $SWWAR_{MJJ}$ and NCR_{JAS} is not strongly influenced by the SAM because the partial correlations between time series $SWWAR_{MJJ}$ and NCR_{JAS} remain 0.55, significant at the 0.05 level after removing the SAM effect in MJJ and JAS. Worthy of note is that the precise role of the SAM on the drying trend in SWWA remains ambiguous and is still an area of ongoing research (Feng et al. 2010b; Cai et al. 2011). Additionally, the physical process driving the observed relationship between the SAM_{JAS} and the NCR_{JAS} remains unclear, and warrants a further investigation in the future.

Therefore, the teleconnection between $SWWAR_{MJJ}$ and NCR_{JAS} is largely independent of the well-known climate drivers. It is known that the global warming has been associated with the poleward expansion of the Hadley circulation and the subtropical dry zone (Lu et al. 2007). The influence of the global warming on the warming SSTs in the Indian–western Pacific and the poleward shift of the $SSHR_{MJJ}$ and $NSHR_{JAS}$, as well as

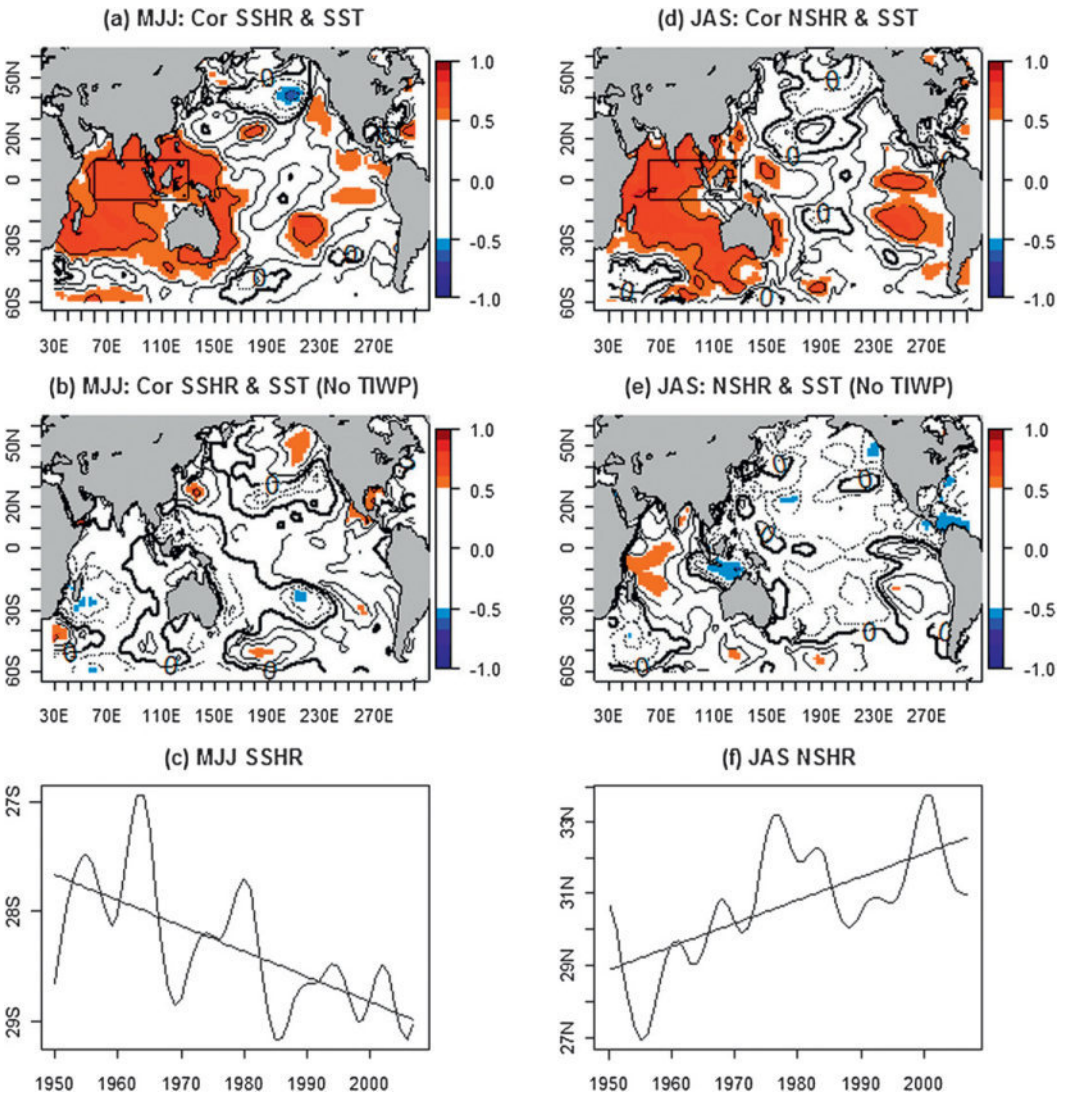

FIG. 11. (a) Correlation map between the SHHR and SST in MJJ on an interdecadal time scale. (b) Partial correlation map between the SHHR and SST by removing the effect of tropical Indian-western Pacific (TIWP) in MJJ on an interdecadal time scale. (c) The time series of the MJJ SSHR index on an interdecadal time scale. (d)–(f) As in (a)–(c), but for NSHR and SST in JAS on an interdecadal time scale, respectively. Only those correlations above the critical value of 0.5, significant at 0.1 level with degree of freedom 7, are marked in colors. Note that the MJJ SSHR has a link to the JAS NSHR on the interdecadal time scale, with a significant correlation of −0.51 with degree of freedom 8, significant at the 0.07 level.

the teleconnection between the rainfall reduction in both SWWA and NC, also warrant further research.

Acknowledgments. We thank three anonymous reviewers whose comments have helped us to improve the original manuscript, and Riyu Lu and Xiaofeng Li for discussion on this research. This work was jointly supported by a project under Australia–China Bilateral Climate Change Partnerships Program, run by the Australian Department of Climate Change and Energy Efficiency, the 973 Program (2010CB950400), the National Natural Science Foundation of China (41030961), and the Indian Ocean Climate Initiative.

APPENDIX A

Maximal Overlap Discrete Wavelet Transform

In this appendix, we give an outline of how to use the MODWT to extract details from the rainfall series over NC and SWWA to study their relationship on the interannual and decadal time scales.

Let **X** be a column vector containing a sequence $X_0, X_1, \ldots, X_{N-1}$ of N observations of a real valued time series (e.g., JJA rainfall series over NC and SWWA, respectively). We assume that the observation X_t was collected at time $t\Delta t$, where Δt is the time interval between the adjacent observations (e.g., $\Delta t = 1$ year for SWWA MJJ rainfall and NC JAS rainfall). Following Percival and Mofjeld (1997), let $h_{1,0}, \ldots, h_{1,L_1-1}$, where $L_1 < N$, be a unit scale wavelet filter from a class of least asymmetric (LA) wavelet filters (Daubechies 1992). This filter sums to 0, has unit, and is orthogonal to its even shifts:

$$\sum_{n=0}^{L_1-1-2t} h_{1,n}h_{1,n+2l} = \begin{cases} 1, & l = 0 \\ 0, & l = 1, 2, \ldots, (L_1 - 2)/2 \end{cases}. \tag{A1}$$

The filter $h_{1,n}$ is associated with the scale $\Delta t = \tau_1 \Delta t$ and is approximately a high-pass filter with a bandpass given by the interval of frequencies $[1/(4\Delta t), 1/(2\Delta t)]$. To define the wavelet filter $h_{j,n}$ for higher scales $2^{j-1}\Delta t$, let

$$H_{1,k} \equiv \sum_{n=0}^{N-1} h_{1,n} e^{-i2\pi nk/N}, \quad k = 0, \ldots, N-1$$

be the discrete Fourier transform (DFT) of the wavelet filter padded with $N - L_1$ zeros. Let $g_{1,n}$ be the corresponding scaling filter, which is defined as

$$g_{1,n} \equiv (-1)^{n+1} h_{1,L_1-1-n} \quad n = 0, \ldots, L_1 - 1. \tag{A2}$$

Let $G_{1,k}$ denote the DFT of zero padded scaling filter. The higher wavelet filters are defined as

$$h_{j,n} \equiv \frac{1}{N} \sum_{k=0}^{N-1} H_{j,k} e^{i2\pi nk/N},$$

where

$$H_{j,k} \equiv H_{1,2^{j-1}k \bmod N} \prod_{l=0}^{j-2} G_{1,2^l \bmod N}. \tag{A3}$$

Elements $h_{j,L_j}, h_{j,L_{j+1}}, \ldots, h_{j,L_{N-1}}$ of this real valued filter are equal to zero when $L_j = (2^j - 1)(L_1 - 1) + 1 < N$. The filter $h_{j,n}$ is approximately a high passband given by the interval of frequencies $[1/(2^{j+1}\Delta t), 1/(2^j \Delta t)]$. Finally, the jth-order scaling filter can be defined as

$$g_{J,n} \equiv \frac{1}{N} \sum_{n=0}^{N-1} G_{J,k} e^{i2\pi nk/N},$$

where

$$G_{j,k} = \prod_{l=0}^{J-1} G_{l,2^l k \bmod N}. \tag{A4}$$

The scaling filter $g_{J,n}$ is approximately a low-pass filter with passband $[0, 1/(2^{J+1}\Delta t)]$.

With these definitions, Percival and Mofjeld (1997) showed that

$$\mathbf{X}_t = \sum_{j=1}^{J} D_j(t) + S_J(t), \tag{A5}$$

where details $D_j = D_j(t)$, an N-dimensional column vector whose elements are associated with changes at the time scale $2^j \Delta t$, $j = 1, \ldots, J$, and the smooth $S_J = S(t)$, which is a similar vector with elements associated with variations at scale $2^{J+1}\Delta t$ and higher. The D_j and S_J series are associated with the zero phase filters, making it possible to line up features in a multiresolution analysis with the original time series. In our study, we have decomposed $\mathrm{SWWAR_{MJJ}}$ and $\mathrm{NCR_{JAS}}$ at interannual and decadal to interdecadal time scales using the decomposed rainfall series by MODWT with $J = 2$. The interannual component is represented by the sum of details (D1 + D2) associated variations at 2–7 years, and the interdecadal component by the smooth S2 with variations longer than 8 years, respectively.

APPENDIX B

The Modified Chelton Method

The modified Chelton method was introduced to test the significance of the correlation between two autocorrelated time series through the adjusted the number of degree of freedom (Pyper and Peterman 1998). The effective number of degrees of freedom, N^{eff}, can be given by the following the theoretical approximation

$$\frac{1}{N^{\mathrm{eff}}} \approx \frac{1}{N} + \frac{2}{N} \sum_{j=1}^{N} \frac{N-j}{N} \rho_{\mathrm{XX}}(j)\, \rho_{\mathrm{YY}}(j), \tag{B1}$$

where N is the sample size and $\rho_{\mathrm{XX}}(j)$ and $\rho_{\mathrm{YY}}(j)$ are the autocorrelations of two sampled time series X and Y. Given N^{eff}, the critical value for the null hypothesis that the correlation between time series X and Y is different from zero at the α significant level can be derived using the t distribution for either one- or two-tailed tests (Zar 1984, p. 309):

$$r_{\mathrm{crit}} = \sqrt{t^2_{\alpha,N^{\mathrm{eff}}} / (t^2_{\alpha,N^{\mathrm{eff}}} + N^{\mathrm{eff}})}. \tag{B2}$$

When the correlation exceeds the critical value r_{crit}, the null hypothesis (i.e., the correlation between series X and Y is zero) must be rejected, and this correlation is considered significant at the corresponding α level. In our study, the correlation between SWWA and NC is 0.82 on the interdecadal time scale is highly significant at the 0.01 level, because it is bigger than the critical value 0.75 at the 0.01 level with the effective number of degrees of freedom $N_{ID}^{eff} = 7$.

REFERENCES

Cai, W., and I. G. Watterson, 2002: Modes of interannual variability of the Southern Hemisphere circulation simulated by the CSIRO climate model. *J. Climate,* **15,** 1159–1174.

——, and T. Cowan, 2006: SAM and regional rainfall in IPCC AR4 models: Can anthropogenic forcing account for southwest Western Australian winter rainfall reduction? *Geophys. Res. Lett.,* **33,** L24708, doi:10.1029/2006GL028037.

——, P. H. Whetton, and D. J. Karoly, 2003: The response of the Antarctic Oscillation to increasing and stabilized atmospheric CO_2. *J. Climate,* **16,** 1525–1538.

——, G. Shi, and Y. Li, 2005: Multidecadal fluctuations of winter rainfall over southwest Western Australia simulated in the CSIRO Mark 3 coupled model. *Geophys. Res. Lett.,* **32,** L12701, doi:10.1029/2005GL022712.

——, P. van Rensch, S. Borlace, and T. Cowan, 2011: Does the southern annular mode contribute to the persistence of the multidecade-long drought over southwest Western Australia? *Geophys. Res. Lett.,* **38,** L14712, doi:10.1029/2011GL047943.

Chang, C. P., Y. Zhang, and T. Li, 2000a: Interannual and interdecadal variations of the East Asian summer monsoon and tropical Pacific SSTs. Part I: Roles of the subtropical ridge. *J. Climate,* **13,** 4310–4325.

——, ——, and ——, 2000b: Interannual and interdecadal variations of the East Asian summer monsoon and tropical Pacific SSTs. Part II: Meridional structure of the monsoon. *J. Climate,* **13,** 4326–4340.

Cheng, Y., U. Lohmann, J. Zhang, Y. Luo, Z. Liu, and G. Lesins, 2005: Contribution of changes in sea surface temperature and aerosol loading to the decreasing precipitation trend in Southern China. *J. Climate,* **18,** 1381–1390.

Dai, A., and T. M. L. Wigley, 2000: Global patterns of ENSO-induced precipitation. *Geophys. Res. Lett.,* **27,** 1283–1286.

Daubechies, I., 1992: *Ten Lectures on Wavelets.* CBMS-NSF Regional Conference Series in Applied Mathematics, Vol. 61, SIAM, 377 pp.

Ding, Y. H., Z. Y. Wang, and Y. Sun, 2008: Inter-decadal variation of the summer precipitation in East China and its association with decreasing Asian summer monsoon. Part I: Observed evidences. *Int. J. Climatol.,* **28,** 1139–1161.

England, M. H., C. C. Ummenhofer, and A. Santoso, 2006: Interannual rainfall extremes over southwest Western Australia linked to Indian Ocean climate variability. *J. Climate,* **19,** 1948–1969.

Feng, J., J. Li, and Y. Li, 2010a: A monsoon-like southwest Australian circulation and its relation with rainfall in southwest Western Australia. *J. Climate,* **23,** 1334–1353.

——, ——, and ——, 2010b: Is there a relationship between the SAM and southwest Western Australian winter rainfall? *J. Climate,* **23,** 6082–6089.

Gong, D., and S. Wang, 1999: Definition of Antarctic Oscillation Index. *Geophys. Res. Lett.,* **26,** 459–462.

——, and C.-H. Ho, 2002: Shift in the summer rainfall over the Yangtze River valley in the late 1970s. *Geophys. Res. Lett.,* **29,** 1436, doi:10.1029/2001GL014523.

Guo, Y., J. P. Li, and Y. Li, 2012: A time-scale decomposition approach to statistically downscale summer rainfall over north China. *J. Climate,* **25,** 572–591.

Hendon, H. H., D. W. J. Thompson, and M. C. Wheeler, 2007: Australian rainfall and surface temperature variations associated with the Southern Hemisphere annular mode. *J. Climate,* **20,** 2452–2467.

Hu, Z.-Z., S. Yang, and R. G. Wu, 2003: Long-term climate variations in China and global warming signals. *J. Geophys. Res.,* **108,** 4614, doi:10.1029/2003JD003651.

IOCI, 2002: Climate variability and change in southwest Western Australia. Indian Ocean Climate Initiative Rep., 34 pp.

Kalnay, E., and Coauthors, 1996: The NCEP/NCAR 40-Year Reanalysis Project. *Bull. Amer. Meteor. Soc.,* **77,** 437–471.

Karoly, D. J., 2003: Ozone and climate change. *Science,* **302,** 236–237.

Li, J., and Q. Zeng, 2002: A unified monsoon index. *Geophys. Res. Lett.,* **29,** 1274, doi:10.1029/2001GL013874.

——, Z. Wu, Z. Jiang, and J. He, 2010: Can global warming strengthen the East Asian summer monsoon? *J. Climate,* **23,** 6696–6705.

——, G. Wu, and D. Hu, 2011a: *Ocean–Atmosphere Interaction over the Joining Area of Asia and Indian-Pacific Ocean and Its Impact on the Short-Term Climate Variation in China.* Vol. 1. China Meteorological Press, 516 pp.

——, ——, and ——, 2011b: *Ocean–Atmosphere Interaction over the Joining Area of Asia and Indian-Pacific Ocean and Its Impact on the Short-Term Climate Variation in China.* Vol. 2. China Meteorological Press, 576 pp.

——, J. Feng, and Y. Li, 2012: A possible cause of decreasing summer rainfall in northeast Australia. *Int. J. Climatol.,* **32,** 995–1005, doi:10.1002/joc.2328.

Li, Y., W. Cai, and E. P. Campbell, 2005: Statistical modeling of extreme rainfall in southwest Western Australia. *J. Climate,* **18,** 852–863.

Lo, F., M. C. Wheeler, H. Meinke, and A. Donald, 2007: Probabilistic forecasts of the onset of the north Australian wet season. *Mon. Wea. Rev.,* **135,** 3506–3520.

Lu, J., G. A. Vecchi, and T. Reichler, 2007: Expansion of the Hadley cell under global warming. *Geophys. Res. Lett.,* **34,** L06805, doi:10.1029/2006GL028443.

Marshall, G. J., 2003: Trends in the southern annular mode from observations and reanalyses. *J. Climate,* **16,** 4134–4143.

——, P. A. Stott, J. Turner, W. M. Connolley, J. C. King, and T. A. Lachlan-Cope, 2004: Causes of exceptional atmospheric circulation changes in the Southern Hemisphere. *Geophys. Res. Lett.,* **31,** L14205, doi:10.1029/2004GL019952.

Meneghini, B., I. Simmonds, and I. N. Smith, 2007: Association between Australian rainfall and the southern annular mode. *Int. J. Climatol.,* **27,** 109–121.

Menon, S., J. Hansen, L. Nazarenko, and Y. F. Luo, 2002: Climate effects of black carbon aerosols in China and India. *Science,* **297,** 2250–2253.

Nan, S., and J. P. Li, 2003: The relationship between the summer precipitation in the Yangtze River valley and the boreal spring Southern Hemisphere annular mode. *Geophys. Res. Lett.,* **30,** 2266, doi:10.1029/2003GL018381.

Nitta, T., and Z.-Z. Hu, 1996: Summer climate variability in China and its association with 500 hPa height and tropical convection. *J. Meteor. Soc. Japan,* **74,** 425–445.

Percival, D. B., and H. O. Mofjeld, 1997: Analysis of subtidal coastal sea level fluctuations using wavelets. *J. Amer. Stat. Assoc.,* **92,** 868–880.

Pitman, A. J., G. T. Narisma, R. A. Pielke, and N. J. Holbrook, 2004: Impact of land cover change on the climate of southwest Western Australia. *J. Geophys. Res.,* **109,** D18109, doi:10.1029/2003JD004347.

Pyper, B. J., and R. M. Peterman, 1998: Comparison of methods to account for autocorrelation in correlation analyses of fish data. *Can. J. Fish. Aquat. Sci.,* **55,** 2127–2140.

Qian, Y., L. R. Leung, S. J. Ghan, and F. Giorgi, 2003: Regional climate effects of aerosols over China: Modeling and observation. *Tellus,* **55B,** 914–934.

Ren, B., R. Lu, and Z. Xiao, 2004: A possible linkage in the interdecadal variability of rainfall over North China and the Sahel. *Adv. Atmos. Sci.,* **21,** 699–707.

Rogers, J. C., and H. Vanloon, 1982: Spatial variability of sea-level pressure and 500-mb height anomalies over the Southern Hemisphere. *Mon. Wea. Rev.,* **110,** 1375–1392.

Saji, N., B. Goswami, P. Viayachandran, and T. Yamagata, 1999: A dipole mode in the tropical Indian Ocean. *Nature,* **401,** 360–363.

Shi, N., and Q. G. Zhu, 1996: An abrupt change in the intensity of the East Asian summer monsoon index and its relationship with temperature and precipitation over east China. *Int. J. Climatol.,* **16,** 757–764.

Smith, T. M., and R. W. Reynolds, 2004: Improved extended reconstruction of SST (1854–1997). *J. Climate,* **17,** 2466–2477.

Thompson, D. W. J., and J. M. Wallace, 2000: Annular modes in the extratropical circulation. Part I: Month-to-month variability. *J. Climate,* **13,** 1000–1016.

Ummenhofer, C. C., A. Sen Gupta, M. J. Pook, and M. H. England, 2008: Anomalous rainfall over southwest Western Australia forced by Indian Ocean sea surface temperatures. *J. Climate,* **21,** 5113–5134.

van Ommen, T. D., and V. Morgan, 2010: Snowfall increase in coastal East Antarctica linked with southwest Western Australian drought. *Nat. Geosci.,* **3,** 267–272.

Wang, B., Z. Wu, J. Li, J. Liu, C.-P. Chang, Y. Ding, and G. Wu, 2008: How to measure the strength of the East Asian summer monsoon. *J. Climate,* **21,** 4449–4463.

——, J. Liu, J. Yang, T. Zhou, and Z. Wu, 2009: Distinct principal modes of early and late summer rainfall anomalies in East Asia. *J. Climate,* **22,** 3864–3875.

Weng, H., K.-M. Lau, and Y. Xue, 1999: Multi-scale summer rainfall variability over China and its long-term link to global sea surface temperature variability. *J. Meteor. Soc. Japan,* **77,** 845–857.

Wu, Z., B. Wang, J. Li, and F.-F. Jin, 2009: An empirical seasonal prediction model of the East Asian summer monsoon using ENSO and NAO. *J. Geophys. Res.,* **114,** D18120, doi:10.1029/2009JD011733.

——, J. Li, Z. Jiang, J. He, and X. Zhu, 2012a: Possible effects of the North Atlantic Oscillation on the strengthening relationship between the East Asian summer monsoon and ENSO. *Int. J. Climatol.,* **32,** 794–800.

——, ——, ——, and T. Ma, 2012b: Modulation of the Tibetan Plateau snow cover on the ENSO teleconnections: From the East Asian summer monsoon perspective. *J. Climate,* **25,** 2481–2489.

Xin, X. G., R. C. Yu, T. J. Zhou, and B. Wang, 2006: Drought in late spring of south China in recent decades. *J. Climate,* **19,** 3197–3206.

Xu, Q., 2001: Abrupt change of the mid-summer climate in central east China by the influence of atmospheric pollution. *Atmos. Environ.,* **35,** 5029–5040.

Yang, F., and K.-M. Lau, 2004: Trend and variability of China precipitation in spring and summer: Linkage to sea-surface temperatures. *Int. J. Climatol.,* **24,** 1625–1644.

Yang, S., and L. Z. Xu, 1994: Linkage between Eurasian winter snow cover and regional Chinese summer rainfall. *Int. J. Climatol.,* **14,** 739–750.

Yatagai, A., and T. Yasunari, 1994: Trends and decadal-scale fluctuations of surface air-temperature and precipitation over China and Mongolia during the recent 40-year period (1951–1990). *J. Meteor. Soc. Japan,* **72,** 937–957.

Yu, R., and T. Zhou, 2007: Seasonality and three-dimensional structure of interdecadal change in the East Asian monsoon. *J. Climate,* **20,** 5344–5355.

——, B. Wang, and T. Zhou, 2004: Tropospheric cooling and summer monsoon weakening trend over East Asia. *Geophys. Res. Lett.,* **31,** L22212, doi:10.1029/2004GL021270.

Zar, J. H., 1984: *Biostatistical Analysis*. Prentice Hall, 718 pp.

Zeng, Q., and J. Li, 2002: On the interaction between Northern and Southern Hemispheric atmospheres and the essence of tropical monsoon (in Chinese). *Chin. J. Atmos. Sci.,* **26,** 207–226.

Zhang, Q., 1999: The variation of the precipitation and water resources in north China since 1880 (in Chinese). *Plat. Meteor.,* **18,** 486–495.

Zhang, Y., T. Li, and B. Wang, 2004: Decadal change of the spring snow depth over the Tibetan Plateau: The associated circulation and influence on the East Asian summer monsoon. *J. Climate,* **17,** 2780–2793.

Zhao, P., and X. Zhou, 2006: Decadal variability of rainfall persistence time and rainbelt shift over eastern China in recent 40 years. *J. Appl. Meteor. Sci.,* **17,** 548–556.

——, S. Yang, and R. Yu, 2010: Long-term changes in rainfall over eastern China and large-scale atmospheric circulation associated with recent global warming. *J. Climate,* **23,** 1544–1562.

Zhou, W., C. Li, and J. C. L. Chan, 2006: The interdecadal variations of the summer monsoon rainfall over South China. *Meteor. Atmos. Phys.,* **93,** 165–175.

Zhu, X., J. He, and Z. Wu, 2007: Meridional seesaw-like distribution of the Meiyu rainfall over the Changjiang-Huaihe River Valley and characteristics in the anomalous climate years. *Chin. Sci. Bull.,* **52,** 2420–2428.